Elsevier Editorial System(tm) for Journal of Alloys and Compounds

Manuscript Draft

Manuscript Number:

Title: Ammonia gas sensing characteristics of V2O5 nanostructures: A combined experimental and ab initio density functional theory approach

Article Type: Full Length Article

Keywords: α-V2O5, para- to ferro- magnetic transition, NH3 adsorption, NH3 sensing, electronic band gap

Corresponding Author: Dr. Amos Adeleke Akande, PhD

Corresponding Author's Institution: University of Limpopo

First Author: Amos Adeleke Akande, PhD

Order of Authors: Amos Adeleke Akande, PhD; Thuto Mosuang, PhD; Cecil N Ouma, PhD; Evans M Benecha, PhD; Tuquabo Tesfamicheal, PhD; Kittessa Roro, PhD; Augusto G Machatine, PhD; Bonex Mwakikunga, PhD

Abstract: A combined experimental and density functional theory study of NH3 gas sensing and adsorption characteristics of α-V2O5 synthesized from hydrated NH4VO3 in CVD at 400 ˚C (in N2 for 12 and 24 h.) is presented. Highly crystalline orthorhombic α-V2O5 nano-rods with dominant (001) and (110) planes/facets nano-rods were observed from XRD, SEM and TEM
characterizations. Using VSM technique, para- to ferro- magnetic transition was observed in the α-V2O5 nanoparticles synthesized at 24 h. Improved gas sensing was observed in the case of paramagnetic α-V2O5 nano-rods (nanoparticles synthesized at 12 h.) compared with the one synthesized at 24 h. Additionally, significant rise in gas sensing response was observed around the metal to insulator transition temperature. Calculation of adsorption of NH3 molecule(s) on (001), (110), (200) and (400) facets showed that (001), (200) and (400) possessed more active sites than (110) surface. DFT calculations were also used to investigate NH3 adsorption on (110) surface of α-V2O5 with the analysis showing exponential decrease in the electronic band gap of the material's surface with the increasing numbers of NH3 loadings.

Prime Novelty Statement

University of Limpopo
Faculty of Science and Agriculture
School of Physical and Mineral Sciences
Department of Physics
Private Bag X1106, Sovenga, 0727, South Africa
Tel: (015) 268 3576, Fax: (015) 268 3529, Email:amos.akande@ul.ac.za

To: Editor-in-Chief, Journal of Alloys and Compounds

Date: 23rd July, 2019

Dear Professor,

Subject: Submission of new manuscript **"Ammonia gas sensing characteristics of V_2O_5 nanostructures: A combined experimental and *ab initio* density functional theory approach"** by A. A. Akande[1*], T. Mosuang[1], C. N. M. Ouma[2], E.M. Benecha[3], T. Tesfamicheal[4], K. Roro[5], A. G. J. Machatine[6], B. W. Mwakikunga[7]

We wish to submit this article for your consideration for peer review and subsequent possible publication in your esteemed journal. Few highlights are worth mentioning.

We have synthesized and characterized nano-rods structure of Orthorhombic α-V_2O_5 for application in gas sensing technology. After thorough measurements and analyses of the material for NH_3 gas sensing, we observed that the material, when prepared at 400 ˚C for 12 hours demonstrated excellent response near the metal- to-insulator transition temperature (MIT) of the material. This enhance NH_3 gas sensitivity effect of V_2O_5 nanomaterial at MIT can greatly impact the production of selective gas sensor technology.

The same material, after modelled via Density Functional Theory showed NH_3 adsorption energy's profile which simulated the experimental sensing results. Reduction in the electronic band gap of the NH_3 adsorbed surface of the material with increasing number of the adsorbed molecules was observed, which is not only new, but also supported the general experimental gas and chemical sensing mechanism. We confirm that this work is original and has not been published elsewhere, neither it is in consideration to be submitted in another journal.

We look forward to the opinion of peers and your consideration to publish this paper in this journal. We hope indeed this paper adds knowledge to the Alloys and Compounds community.

Yours sincerely

Dr. A. A Akande

Ammonia gas sensing characteristics of V_2O_5 nanostructures: A combined experimental and *ab initio* density functional theory approach

A. A. Akande[1,2*], T. Mosuang[1], C. N. M. Ouma[3], E.M. Benecha[4], T. Tesfamicheal[5], K. Roro[6], A. G. J. Machatine[7], B. W. Mwakikunga[8,9]

[1]University of Limpopo, Department of Physics, P/Bag X1106, Sovenga 0727, South Africa

[2]CSIR Nextgen Enterprises and Institutions, P O Box 395, Pretoria 0001, South Africa

[3]HySA-Infrastructure, North-West University, Faculty of Engineering, Private Bag X6001, Potchefstroom, South Africa, 252

[4]School of Interdisciplinary and Graduate Studies, University of South Africa, UNISA 0003, Pretoria, South Africa

[5]Science and Engineering Faculty, Queensland University of Technology 2 George Street, Brisbane, 4000, QLD Australia

[6]R&D core-Energy, Council for Scientific and Industrial Research, P O Box 395, Pretoria 0001, South Africa

[7]Department of Physics, University of Pretoria, Pretoria, 0002, South Africa

[8]DST/CSIR National Centre for Nano-Structured Materials, P O Box 395, Pretoria 0001, South Africa

[9] Department of Physics, Tshwane University of Technology, Pretoria, South Africa

Abstract

A combined experimental and density functional theory study of NH_3 gas sensing and [1]adsorption characteristics of α-V_2O_5 synthesized from hydrated NH_4VO_3 in CVD at 400 ˚C

[1] Author to whom correspondence is to be addressed:
*Amos Adeleke Akande Email address: amos.akande@ul.ac.za

(in N_2 for 12 and 24 h.) is presented. Highly crystalline orthorhombic α-V_2O_5 nano-rods with dominant (001) and (110) planes/facets nano-rods were observed from XRD, SEM and TEM characterizations. Using VSM technique, para- to ferro- magnetic transition was observed in the α-V_2O_5 nanoparticles synthesized at 24 h. Improved gas sensing was observed in case of paramagnetic α-V_2O_5 nano-rods (nanoparticles synthesized at 12 h.) compared with the one synthesized at 24 h. Additionally, significant rise in gas sensing response was observed around the metal to insulator transition temperature. Calculation of adsorption of NH_3 molecule(s) on (001), (110), (200) and (400) facets showed that (001), (200) and (400) possessed more active sites than (110) surface. DFT calculations were also used to investigate NH_3 adsorption on (110) surface of α-V_2O_5 with the analysis showing exponential decrease in the electronic band gap of the material's surface with the increasing numbers of NH_3 loadings.

Keywords: α-V_2O_5, para- to ferro- magnetic transition, NH_3 adsorption, NH_3 sensing, electronic band gap

1. Introduction

Vanadium pentoxide (V_2O_5) bulk and nanostructures have been extensively investigated for their catalysis, lithium ion battery, electrochromic and gas sensing applications over the years [1-6]. Their extensive applications can be attributed to the layered structural property of V_2O_5 which makes it easy to embed both organic and inorganic molecules [7-8]. Orthorhombic V_2O_5 belongs to space group, P*mmn* (D_{2h}^{13} No. 59) with lattice parameters a = 11.510 Å, b = 3.563 Å and c = 4.369 Å. Under ambient conditions, orthorhombic V_2O_5 is usually

thermodynamic favoured when b and c lattice parameters are flipped hence its use for room temperature application [9 -14].

Orthorhombic V_2O_5, like other vanadium oxide polymorphs, exhibits a Mott Hubbard's metal-to-insulator transition (MIT) at temperature of ~ 375 °C [4] with no structural change making it attractive for many applications. Orthorhombic V_2O_5 contains two atoms of vanadium V located at same 4*f* Wyckoff position with cite symmetry C*s* [14-15], and three atoms of oxygen at different Wyckoff positions and site symmetries (two at 4*f* Wyckoff position with site symmetry C*s* and one at 2a Wyckoff position with cite symmetry of C_2v [14].) Additionally, the coordination of atoms in V_2O_5 has been proven as useful in evolving catalytic reactions, rechargeable batteries among as other novel applications [14 -18].

As chemical probe, V_2O_5 materials have been used for gas sensing applications due to its ability to adsorb (desorb molecules including ammonia, hydrogen, nitrogen oxides, carbon oxides, hydrocarbon and many volatile organic molecules [4-6, 19-23]. These studies have also observed that it is the V_2O_5 atomic structure, valence state and oxygen coordination and vacancy that accounts for its gas sensing ability. However, similar to its metal oxide counterparts, the need for improved sensitivity and selectivity has hampered the design and manufacture of working sensing devices. The aim of this current work is to investigate theoretically and experimentally the surface properties of V_2O_5 for ammonia gas sensing. Theoretical calculations of adsorption energies, charge density differences and electronic band structure analysis of different ammonia-adsorbed cleaved surfaces have been considered as selectivity indicators. The typical coordination of Orthorhombic V_2O_5 structure, represented in Fig. (1a), and the *ab initio* simulated structure in Fig. (1b) (courtesy of materials project and BIOVIA materials studio) showed the chain and layer characteristics of the material. Each oxygen atoms possessed different coordination with the centred atom;

vanadium, having different bond lengths and Brönsted sites resulting to three structurally different lattice oxygen [22].

2. Materials and Methods

2.1 Synthesis and characterization of V_2O_5 nanorods

Following the decomposition of precursor NH_4VO_3 and phase evolution studies of vanadium oxides reported in our previous manuscript [4], thermodynamic and structural parameters of V_2O_5 nanostructure was selected for this study. Here, an amount of NH_4VO_3 was heat-treated during solid-state reaction in a furnace at 400 °C for 12 and 24 h sampling time in nitrogen atmospheric conditions. The resulting nano-powders were characterized to extract their crystal structural information using Panalytical XPERT PRO PW3050/50 diffractometer with CuKα radiation (45 kV, 400 mA, λ = 0.1540598 nm and $5^{o} \leq 2\theta \leq 90^{o}$). Microstructure studies were carried out using JEOL 2100 Transmission Electron Microscopy (TEM) (from Tokyo Japan) equipped with a LaB6 filament and a Gartan U1000 camera of 2028 × 2028 pixels, and a high quality in-built Energy dispersive X-ray spectroscopy (EDS) set-up. Magnetic characterization was performed using Lakeshore 735 vibrating sample magnetometer (VSM) at room temperature.

2. 2 Gas sensor fabrication and testing

The gas sensor fabrication and testing were carried out using KSGA565 KENOSISTEC instrument from Italy. The sensing electrodes were prepared by ultrasonically dispersing the nanoparticles in the organic solvent for 30 minutes and later drop casting the solution onto an Al_2O_3-Pt interdigitated electrode (IDE) with heating terminal at the reverse side. The sensor's electrodes were dried at~70 ˚C in an electric oven for 1 h to ensure thin film deposition of the

nanoparticles. Finally, the sensing data were acquired by monitoring changes in electrical currents (i.e electrical current of the sensor material when in the presence of the analyte gas minus the one in the absence of such a gas) for various concentrations of the target analyte or gas molecules using the Keithley pico-meter source meter. Figure 2 present the schematic arrangement of the sensing peripherals.

The sensor's response is determined by measuring the voltage changes of the load resistance. According to the figure, the electronic circuit displays of the gas sensor's element showed R_L, which is the load resistor connected in series with the sensor's element ($R_L = (V\text{-}V_S)/I$) and with a value of 5MΩ. V, is the voltage on the R_L, $V_S = V_C - IR_L$, represent the sensor's signal voltage. V_C is a constant voltage applied on the R_L and sensor's element (having a value of 3V in this experiment) and finally, R_S is the sensor's resistance ($R_S = V_S/I$).

2.3 Computational details

First principles thermodynamic *ab initio* calculations were performed within the formalism of density functional theory (DFT), as implemented in the CASTEP [24]. All calculations adopted the Perdew-Burke-Ernzerhof generalized gradient approximation [25] the (GGA-PBE) functional for treating the exchange-correlation effects, while valence-core interactions were approximated by the Vanderbilt ultrasoft pseudopotentials [26]. Full relaxation and geometry optimization and electronic structure calculations were carried out using a bulk orthorhombic V_2O_5 unit cell (space group P*mmn* (D_{2h}^{13} No. 59)) with lattice parameters a = 11.510 Å, b = 3.563 Å and c = 4.369 Å. Adsorption calculations were performed using adsorption locator [26 - 27] by cleaving (001), (110), (200) and (400) surfaces (all chosen based on experimental XRD characterization results in Fig. 3) of the optimized V_2O_5 primitive unit cell. For each of the cleaved surfaces, a 2×2 supercell was constructed to allow large adsorption surface area. A uniform vacuum spacing of 20 nm was allowed in the z-

direction to minimize surface-image interaction, after which fully relaxed NH_3 molecules were allowed to interact with each of the surfaces.

3. Results and Discussion

X-ray diffraction spectra of the sample annealed at 400 °C for 12 and 24 h. are shown in Fig. 3. According to the ICDD (the institute of crystallographic and diffraction database) with powder diffraction number of PDF #41-1426, both samples showed highly crystalline orthorhombic phase of V_2O_5 particles. The spectral showed Braggs positions with strong correlation with the V_2O_5 structure when matched in the Jade 6 software. Among the diffraction planes present in the samples, (001) and (110) were found to be dominant with strong intensities indicating that the majority of the nanoparticles are oriented in (001) and (110) planes or facets. Average crystallite size and micro/nano strain analyses of the nanoparticles were achieved using Debye Scherrer's and Williamson-Hall's relations and shown in Table 1. This analyses showed that the sample annealed at 24 h. has larger crystallites with bigger strain compared with the one annealed for 12 h. This calculation is clearly supported by the XRD patterns and the inserted magnified peak of the (200) plane in Fig. 3 which showed that the sample annealed for 24 h. shifted to the higher angle by about 0.15°. Physical consequences where such observation could be originated from are changes in lattices parameters (distortion in the crystal structure) and strain gradient, which is caused by the stress on the nanoparticles. This showed that the effect of the long period of annealing has slightly deformed the nanoparticles prepared for 24 h. The morphology characterization by SEM and TEM in Fig 4 showed nano rod particles formation from bundles of sheets and platelets of V_2O_5 structure. The sample prepared for 24 h. showed more crystallinity in its high resolution TEM image (Fig. 4 (d)) and the elemental technique, EDX spectrum which clearly revealed the constituents and qualities of the chemicals involved in the materials is presented in Fig 4 (e).

The M-H hysteresis curve of the samples and the summaries of the magnetic analysis were presenrted in Fig. 5 and Table 1 showed an improved magnetic properties like remanence magnetization, saturation magnetization and magenetic coecivity for the sample annealed for 24 h. Even though, both samples generally demostrated superparamagnetic characteristics in the M-H curve by showing narrow hysteresis widths and saturation at the tips of the curve countrary to the usual paramagnetic behavioure of vanadium oxide, the sample annealed for 24 h. displaed superior magnetic properties. This further show a transition in the case of the sample annealed for 24 h. form parallel non-interacting and randomly oriented spins (paramagnetic state) to slightly alignment of moments (say ferromagnetic state).

The gas sensing characteristics of the samples analysed thoroughly as described in the section 2.2 are presented in Fig. 6 and 7. The dynamic response and recovery chemiresistive signals of NH_3 gas on both samples presented in Fig. 6 demonstrated promising sensing property for practical device development. Fig. 6 (a) is the signals acquired at the operating temperature of 350 °C while Fig. 6 (b) is the one taken at 400 °C. It is generally observed that the sample prepared for 12 h. showed a slight superiority in response over the sample annealed for 24 h. especially at the high temperature. This is summarized in the sensor's responses and concentration profile and 60 ppm response versus operating temperature in the Fig. 7 and 8 respectively. The sensor response in this work is defined as the relative change in the electrical property (current or resistance) of the V_2O_5 nanoparticles in the presence or absence of a gas analyte [28]. This slightly low sensing response displays in the case of the sample prepared at 24 h. could be linked to its structural deformation and magnetic transition. Theoretically, one would expect magnetic properties and sensing characteristics to share an inverse relationship since a material with well-aligned or oriented magnetic spins are likely to possess less surface defect, which normally play an important role in gas and chemical sensor's performance. It is also observed in Fig. 6 that the introduction of gas analyte resulted

in an increasing current (decreasing resistance) through the sensors and it's withdraw decreases current (increases resistance) thereof. This is certainly true for the n-conductivity type; V_2O_5 nanomaterial, and the reducing gas; NH_3 molecule [29]. Thus, the following processes are possible; when the V_2O_5 nanoparticles surface is exposed to the synthetic air present in the gas-sensing chamber, the materials surface would undergo a chemisorption process that will lead to the formation of adsorb oxygen (ionic species of oxygen) at the surface of the material. This process would rob the semiconductor of its conduction band electrons leading to decrease in current (increase in resistance) of the material. Now, when the material is exposed to NH_3, a reducing gas and an electron donor [19 - 20, 28 - 31], the Fermi level of the material will shift towards the conduction band edge of the material leading to an increase in current and decrease in resistance. However, when the material is disengaged from NH_3 gas exposure, a reverse process would take place. The temperature dependent sensing response profile in Fig. 8 confirms Mott Hubbard's metal-to-insulator transition characteristics of V_2O_5 by exhibiting low response below 375 ˚C and high response above this transition temperature.

Charge transfers and distributions, from DFT calculations, on V_2O_5 structure provided vital information on NH_3 gas sensing characteristics of the V_2O_5. Figures 9, 10 and 11 shows the adsorption of NH_3 molecule (s) and V_2O_5 interface and the charge density distribution in the surface-adsorbate system. As seen in Figs. 9 and 10, there was strong surface–adsorbate interaction with Fig. 9 showing the accumulation of charges on the surface of α-V_2O_5 and depletion of it thereof from NH_3 molecules. The adsorption energy as a function of the number of NH_3 molecules was then obtained with the adsorption defined as;

$$E_a = E_{system} - E_{surface} - E_{adsorbate} \quad (1)$$

where E_{system} represents the total energy of the optimized V_2O_5 system, $E_{surface}$ is the total energy of the clean V_2O_5 surface and $E_{adsorbate}$ is the energy of the NH_3 gas. Negative (positive) values for E_a imply an exothermic reaction [32 – 34]. The calculated adsorption energies were all negative indicating that the surface-adsorbate systems were not only stable but also that the adsorption process was exothermic. From Fig. 11 (a), a decreasing linear pattern in the calculated adsorption energy per NH_3 is presented, showing that NH_3 exhibited less attraction (attractive force) with the increase in the numbers of NH_3 molecules. The normalized profile of adsorption energy per NH_3 in Fig 11 (b) indicated that the (001), (200) and (400) surface have more active sites compared to the (110) surface. This profile also showed that the adsorption pattern is of Langmuir adsorption type, which simulated the actual experimental sensing in Fig 7.

The DFT calculated band structures are presented in Figures 12 and 13 for systems with and without NH_3 adsorption. Figure 12 is the typical electronic band structure of the adsorbed NH_3 molecule(s) on V_2O_5 (110) surface. From Fig. 13, a band gap reduction from ~ 2.2 eV of the clean bulk V_2O_5 system to about around 0.240 eV in the NH_3 adsorbed V_2O_5 (110) surface, was observed. This observation confirms the proposed sensing mechanism above that, NH_3 molecule(s) acts as electron donor(s) by increasing the electron concentration and shifting the Fermi level towards the conduction band edge. The band gap decreased exponentially with the increase in the number of adsorbed NH_3 molecules until it reached saturation around 12 NH_3 molecule loadings. This feature does not only corroborate the experimental response versus NH_3 concentrations (Fig. 7) but also the calculated adsorption energy per NH_3 molecules (Fig. 11).

4. Conclusions

In summary, we have synthesized and characterized an orthorhombic α-V_2O_5 nano-rods structure and also modelled the system so as to study the NH_3 gas sensing and adsorption characteristics of the material. The crystallite sizes and micro/nano strain analyses of the material from XRD spectra showed that the sample prepared for 24 h is slightly deformed compared the one prepared for 12 h. This is also supported by the improvement in its magnetic properties as characterized by the VSM technique. The XRD spectral also showed that the (001) and (110) planes of the materials are dominant t with high degree of crystallinity. The NH_3 gas sensing characteristic of the sample composed of paramagnetic state, that is the one prepared for 12 h. demonstrated high responses compared with the sample prepared for 24 h. These sensors showed significant rise in responses around the metal to insulator transition (MIT) temperature of the V_2O_5 material. The adsorption energies calculations of NH_3 gas molecule on orthorhombic α-V_2O_5 (110) cleaved surfaces indicated that the NH_3 molecules minimized their energies greatly on (001), (200) and (400) than (110) plane by exhibiting less energy. The corresponding adsorption energies per NH_3 molecules against number of NH_3 molecules simulated the experimentally measured response pattern. Finally, the DFT calculated electronic band structure of the NH_3 adsorbed α-V_2O_5 (110) surface showed that the electronic band gap of the material's surface decreased exponentially with the increasing numbers of NH_3 molecules.

5. Acknowledgements

This work was funded by National Research Foundation through the Innovation Post-Doctoral Fellowship Grant of A. A. Akande, (Unique Grant No: 116749). Authors also thank CHPC for computational resources and CSIR for experimental facilities.

6. References

[1] B. Tepper, B. Richer, A. C. Dupuis, H. Kuhlenbeck, C. Hucho, P. Schilbe, M. A, Yarmo, H. J. Freund, Adsorption of molecular and atomic hydrogen on vacuume cleaved V_2O_5 (001) Surf. Sci. 496, (2002), 64-72

[2] M.C. Rao, Vanadium Pentoxide Cathode Material for Fabrication of All Solid State Lithium-Ion Batteries - A Case Study, Res. J. Recent Sci., 2, 3, 67-73, (2013).

[3] C.G. Granqvist, Electrochromic tungsten oxide films: Review of progress 1993- 1998, Solar Energy Mat. Solar Cells 60, 201- 262, (2000)

[4] A.A. Akande, E.C Linganiso, B.P Dhonge, K.E. Rammutla, A. Machatine, L. Prinsloo, H. Kunert, B.W. Mwakikunga, Phase Evolution of vanadium oxides obtained through temperature programmed calcinations of ammonium vanadate in hydrogen atmosphere and their humidity sensing, J. Mat. Chem. Phys. 151, 206, (2015)

[5] A. A Akande, A. G. J. Machatine, B. Masina, G. Chimowa, B. Matsoso, K. Roro, M-M Duvenhage, H. Swart, S.S. Ray, B.W. Mwakikunga, Blue- and red- shifts of V_2O_5 phonons in NH_3 environment by in situ Raman Spectroscopy, J. Phys. D: Applied Physics (2017) 51 (1), 105106.

[6] J. Huotari, A.L. Spetz, J. Lappalainen, Gas Sensing Properties of Pulsed Laser Deposited Vanadium Oxide Thin Films, The 14th International Meeting on Chemical Sensors, IMCS (2012).

[7] S. Surnev, M. G. Ramsey, F. P. Netzer, Vanadium oxide surface studies, Prog. Surf. Sc. **73**, 4-8, (2003) 117-165

[8] S. Zavahir, Q. Xiao, Sarina S. Jian Zhao, S. Bottle, M. Wellard, J. Jia, L. Jing, Y. Huang, J. P. Blinco, H. Wu, H. Y. Zhu, Selective Oxidation of Aliphatic Alcohols using Molecular Oxygen at Ambient Temperature: Mixed-Valence Vanadium Oxide Photocatalysts, ACS Catal., 6, 3580−3588, (2016)

[9] M. Imada, A. Fujimori, Y. Tokura, Metal-insulator transitions, Rev. Modern Phy. **70**, 4, (1998).

[10] U. Schwingenschlögl, V. Eyert, The vanadium Magnéli phases V_nO_{2n-1}, Ann. Phys. (Leipzig) 13, 9, 475 (2004).

[11] P. Kiria, G. Hyettb, R. Binions, Solid-state thermochromic materials, Adv. Mat. Lett. 1, 2, 86 – 105, (2010).

[12] V Eyert, The metal-insulator transitions of VO_2: A band theoretical approach, Ann. Phys. (Leipzig) 11, 9, 1-61 (2002).

[13] M.C. Rao, Structural Stoichiometry and Phase Transitions of MoO_3 Thin Films for Solid State Microbatteries, Res. J. Recent Sci., 2, 3, (2013).

[14] S. Laubach, P. C. Schmidt, A. Thiben, F. J. Fenandez-Madrigal, Q. Wu, W. Jaegemann, M. Klemm, S. Horn, Theoretical and Experimental determination of the electronic structure of V_2O_5, reduced V_2O_{5-x} and sodium intacalated NaV_2O_5, *Phys Chem Chem Phys* 9, 2564 (2007)

[15] T. Schmitt, A. Augustsson, J. Nordgren, L.-C. Dudaa, J. Höwing, T. Gustafsson, U. Schwingenschlögl, V. Eyert, Electronic structure of Li-inserted V_6 O_{13} battery cathodes: Rigid band behavior and effects of hybridization, App. Phys. Let. 86, 064101, (2005)

[16] P. Hejduk M. Witko K. Hermann, Electronic Structure of Unsaturated V2O5(001) and (100) Surfaces: Ab Initio Density Functional Theory Studies, Top. Catal (2009) 52:1105–1115

[17] A. Chakrabarti, K. Hermann, R. Druzinic, M. Witko, F. Wagner, and M. Petersen, Geometric and electronic structure of vanadium pentoxide: A density functional bulk and surface study, Phy. Rev. B. 59, 16, 10 589 (1999)

[18] X. Yin, A. Fahmi, H. Han, A. Endou, S. Salai Cheettu Ammal, M. Kubo, K. Teraishi, A. Miyamoto, Adsorption of H_2O on the V_2O_5 (010) Surface Studied by Periodic Density Functional Calculations, J. Phys. Chem. B 1999, *103*, 3218-3224

[19] A. A. Akande, B. W. Mwakikunga, K. E. Rammutla, A. Machatine, Larger Selectivity of the V_2O_5 Nano-particles Sensitivity to NO_2 than NH_3, *Sens & Tran* 192, 9, (2015)

[20] A. A. Akande, K. E. Rammutla, B. P. Dhonge, A. G. J. Machatine, and B. W. Mwakikunga, Room temperature Methane (CH_4) sensing by vanadium oxide (VO_x) nanoparticles, Adv. Sci. Lett. 22, 901-904 (2016)

[21] Yuxiang Qin, Guangtao Fan, Kaixuan Liu, Ming Hu, Vanadium pentoxide hierarchical structure networks for high performance ethanol gas sensor with dual working temperature characteristic, Sen and Act. B 190 (2014) 141– 148

[22] T. Yang, H. Yu, B. Xiao, Z. Li, M. Zhang, "Enhanced 1-butylamine gas sensing characteristics of flower-like V_2O_5 hierarchical architectures" J. Alloy and Compounds 699 (2017) 921 – 927.

[23] X. Yin, H. Han, I. Gunji, A. Endou, S. S-C. Ammal, M. Kubo, A. Miyamoto, NH_3 Adsorption on the Bronsted and Lewis Acid Sites of V_2O_5 (010): A periodic density Functional Study, J. Phy. Chem. B 103, 4701 - 4706 (1999)

[24] S. J. Clark, M. D. Segall, C. J. Pickard, P. J. Hasnip, M. J. Probert, K. Refson, M. C. Payne, Z. Kristallogr, First Principles methods using CASTEP 220, 567, (2005)

[25] J. P. Perdew, K. Burke, and M. Ernzerhof, Generalized Gradient Approximation Made Simple, Phys. Rev. Lett. 77, 3865 (1996).

[26] D. Vanderbilt, Soft self-consistent pseudopotentials in a generalized eigenvalue formalism Phys. Rev. B 41, 7892 (1990).

[27] J. Ruiyu, L. Dengyang, C. Chao, Zhu Tao, Y. Fanfan, Z. Jinhong, Adsorption simulation of sulfur oxide on the surface of metal, J. Ch. Pharm. Res., 2014, 6(3):949-954

[28] Bonex W. Mwakikunga, Sarah Motshekga, Lucky Sikhwivhilua,, Mathew Moodley, Manfred Scriba, Gerald Malgas, A. Simo, B. Sone, M. Maazad,e, Suprakas Sinha Ray, A classification and ranking system on the H_2 gas sensing capabilities of nanomaterials based on proposed coefficients of sensor performance and sensor efficiency equations, Sen. and Act. B 184 (2013) 170– 178

[29] K. Watchakun, T. Samerjai, N. Tamaekong, C. Liewhiran, C. Siriwong, V. Kruefu, A. Wisitsoraat, A. Tuantranont, and S. Phanichphant, Semiconducting metal oxides as sensor for environmentally hazardous gases, Sen. Act. B. 160, 580-591 (2011).

[30] A. A. Khaleed, A. Bello, J. K. Dangbengnon, D. Y. M omodu, M. J. Madito, F. U. Ugbo, A. A. Akande, B. P. Dhonge, O. Olaniyan, B. W. Mwakikunga, N. Manyala, "Effect of activated carbon on the enhancement of CO sensing performance of NiO" J. Alloy and Compounds 694 (2017) 155 – 162.

[31] C. Zhai, Q. Zhao, K. Gu, D. Xing, M. Zhang, "Ultra-fast response of trimethylamine gas sensors using a MOF-based ZnO/$ZnFe_2O_4$ structures" J. Alloy and Compounds 784 (2019) 660 – 667

[32] M-F. Ng, M. K. Teo, K. H. Lim, L. Zhou, M. B. Sullivan, S-W. Yang, Towards tuning of surface properties by atomic and molecular adsorption on boron-terminated

cubic boron nitride (111) surface: A first-principles study**,** Diamond & Related Mat. 17 2048-2053, (2008).

[33] V. V. Kulish, M-F. Ng, O. I. Malyi, P. Wu, Z. Chen, Enhanced Li Adsorption and Diffusion in Single-Walled Silicon Nanotube: An ab Inito Study, Chem. Phys. Chem. 14, 6 (2013) 1161-1167

[34] O. Leenserts, B. Partoens, F. M. Peeters, Adsorption of H_2O, NH_3, CO, NO_2 nad NO: A first-principle study, Phy. Rev. B 77, (2008), 125416

Table Captions

Table 1: Summary of crystallite size, strain and magnetic properties of the nanopowders samples prepared at 12 and 24 h.

Figure Captions

Fig 1: a) Local coordination of vanadium and oxygen atoms. The grey and red ball(s) are the V and O atoms respectively. O_v – vanadyl oxygen, O_b – bridge oxygen and O_c – chain oxygen respectively. (b) Orthorhombic crystal structure.

Fig. 2: Schematic diagram of KSGA565 KENOSISTEC sensing station illustrating how the gas sensing measurement was performed.

Fig. 3. (a) XRD spectral of the nanopowders samples prepared at 12 and 24 h. Insert is the magnified spectral of the diffraction plane (200).

Fig. 4. SEM and TEM profiles of the nanopowders prepared at 12 and 24 h respectively, (a) and (b); SEM, (c) and (d); TEM, (e) is the representative EDX spectrum of the samples.

Fig. 5. VSM profiles of the nanopowders samples prepared at 12 and 24. Insert is the magnified image of Fig. 2.

Fig. 6. Conductometric NH_3 sensing signal of the samples prepared at 12 and 24, (a) operating temperature of 350 ˚C, (b) operating temperature of 400 ˚C.

Fig. 7. Response profiles as a function of different gas concentrations.

Fig. 8. Response versus operating temperature of 60 ppm concentration of NH_3.

Fig. 9. Electron density difference of V_2O_5 (110) cleaved surface when exposed to NH_3 molecules. Blue shading shows charge accumulation while the yellow shading shows charge depletion.

Fig. 10. Adsorption of NH_3 molecules (in particular for five NH_3 molecules) on V_2O_5 planes (a) (001), (b) (110), (c) (200) and (d) (400).

Fig. 11. (a) Calculated adsorption energy versus number of NH_3 molecules, (b) plot of absolute values of adsorption energies per molecule versus number of NH_3 molecules.

Fig. 12. Electronic band structure of V_2O_5 (110) cleaved surface with adsorbed NH_3 molecules, (a) with 3 NH_3 adsorbed molecules and (b) with 15 NH_3 adsorbed molecules.

Fig. 13. Summary of the calculated electronic band gaps versus number of NH_3 molecules of NH_3 adsorbed V_2O_5 (110) surface

Highlights

- Para- to ferro- magnetic transition behaviour of the Orthorhombic α-V_2O_5 nano-rods particles
- Excellent NH_3 gas response property in the vicinity of α-V_2O_5's metal- to- insulator transition temperature
- Observation of inverse relationship of magnetic and NH_3 sensing property of α-V_2O_5 nano-rods particles
- Correlation of DFT adsorption energy's profile and the actual experimental sensing response of α-V_2O_5
- Reduction in the surface electronic band gap with increasing number of adsorbed NH_3 molecules

Table 1: Summary of crystallite size, strain and magnetic properties of the nanopowders samples prepared at 12 and 24 h.

Samples	Particle Size (nm)	Strain	Saturation Magnetization (*Ms*) (emu/g)	Remanence Magnetization (*Mr*) (emu/g)	Coercivity, (Hci) (Oe)
12 hrs	66	3.547E-04	0.427	0.029	84.658
24 hrs	72	3.786E-04	0.724	0.213	292.420

Figure 1

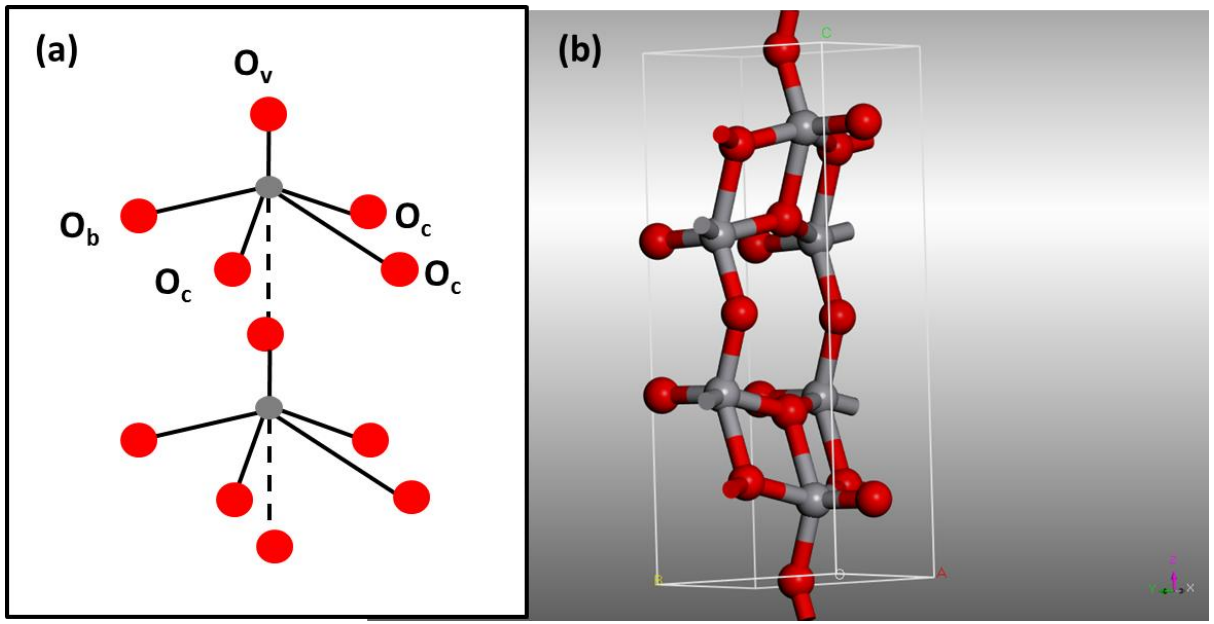

Figure 2

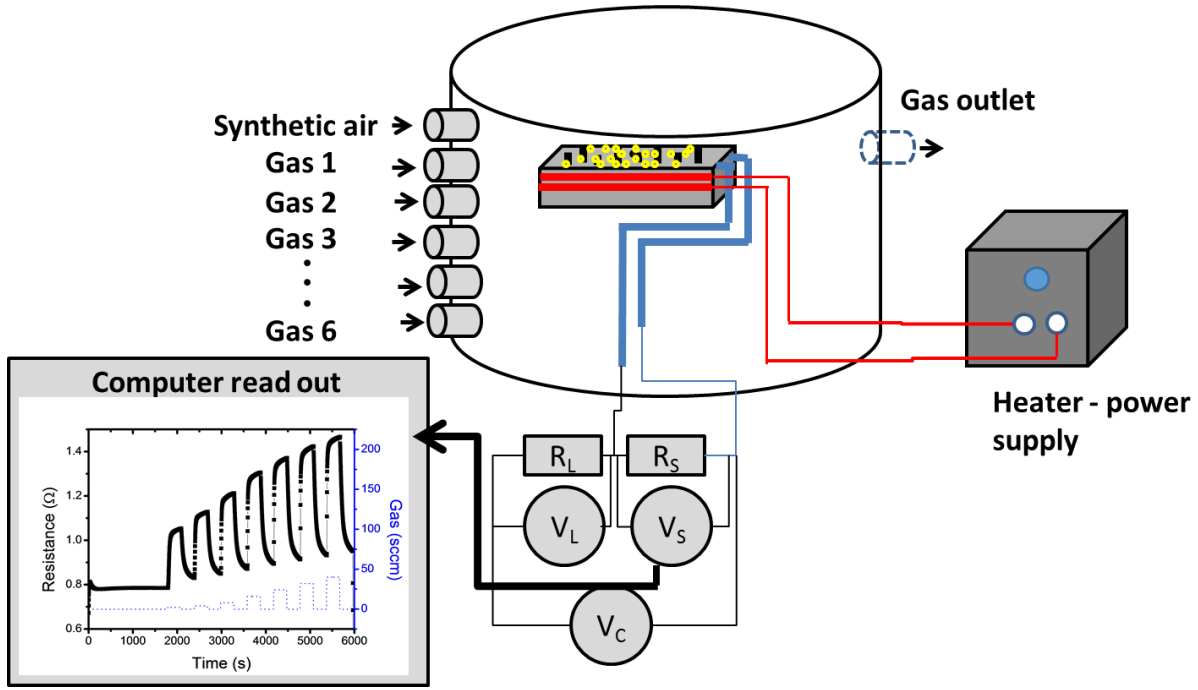
Synthetic air
Gas 1
Gas 2
Gas 3
Gas 6
Gas outlet
Heater - power supply
Computer read out
Resistance (Ω)
Gas (sccm)
Time (s)
R_L
R_S
V_L
V_S
V_C

Figure 3

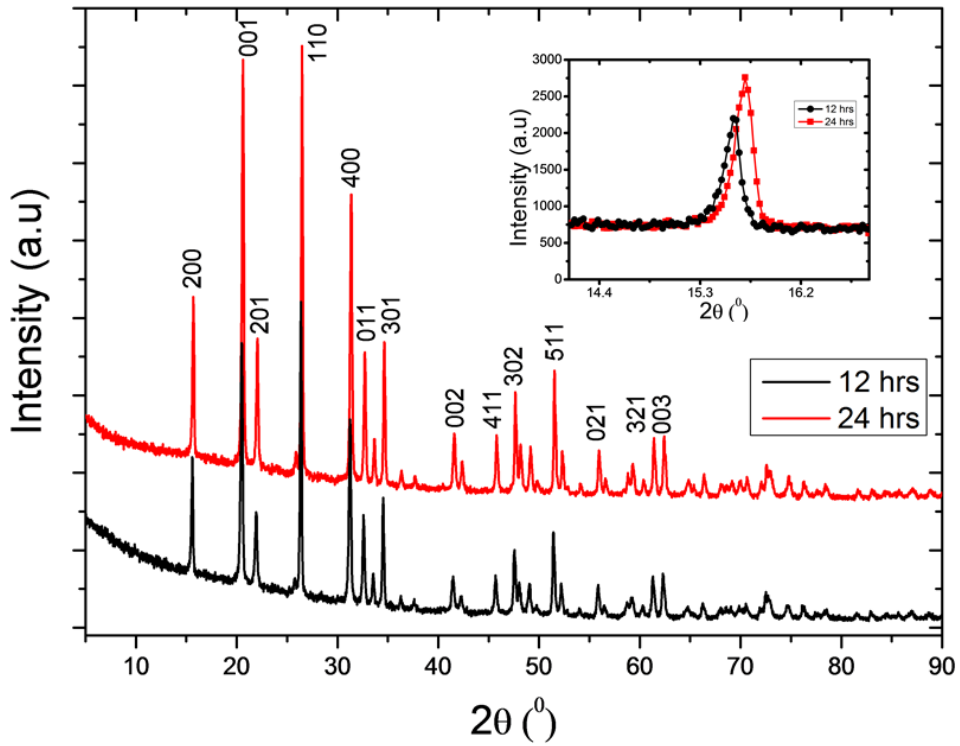
Intensity (a.u)
2θ (0)
200
001
201
110
400
011
301
002
411
302
511
021
321
003
12 hrs
24 hrs
Intensity (a.u)
2θ (0)
12 hrs
24 hrs

Figure 4

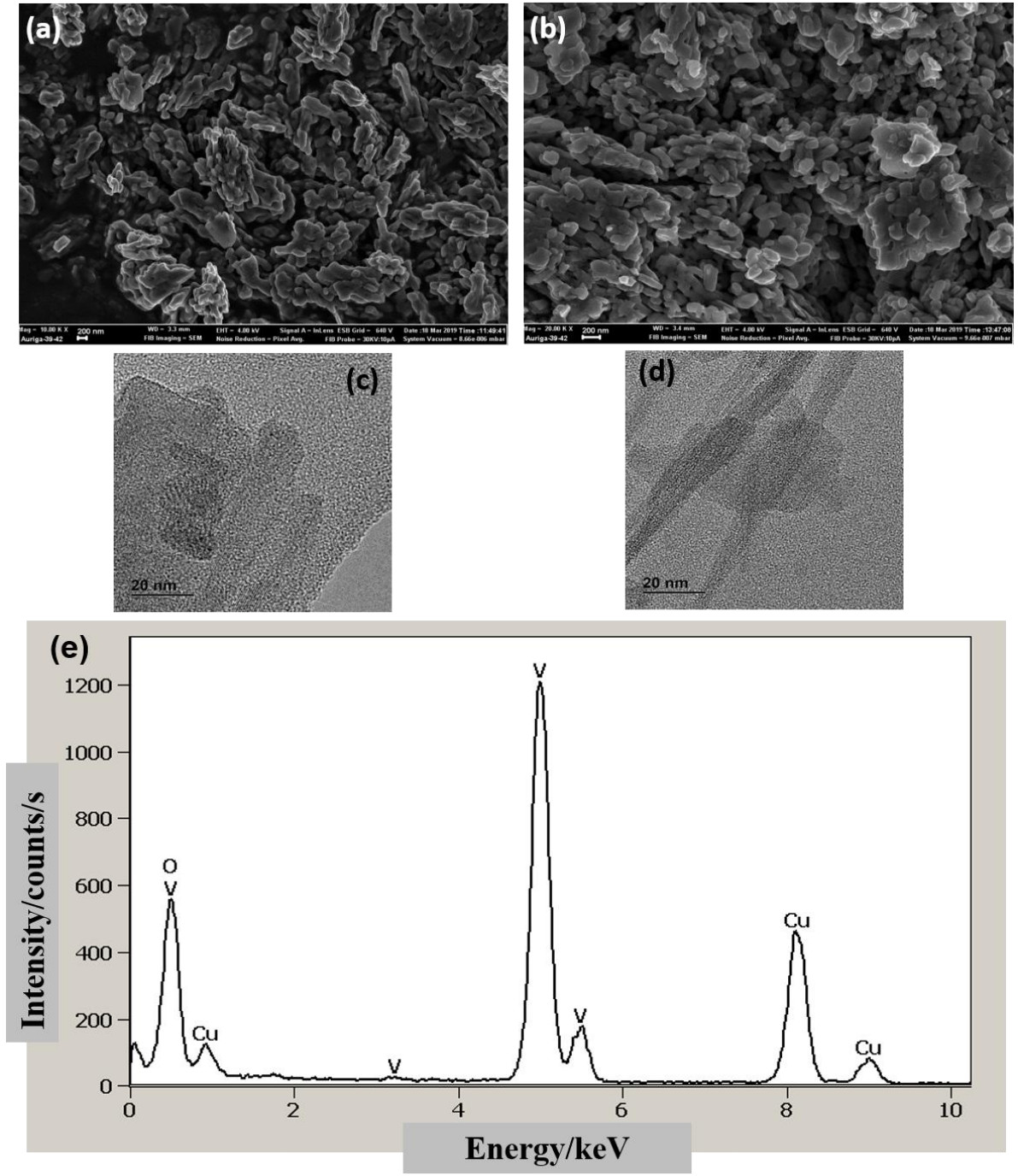
(a)
(b)
(c)
20 nm
(d)
20 nm
(e)
Intensity/counts/s
Energy/keV
O
V
Cu
V
V
Cu
Cu
0
200
400
600
800
1000
1200
0
2
4
6
8
10

Figure 5

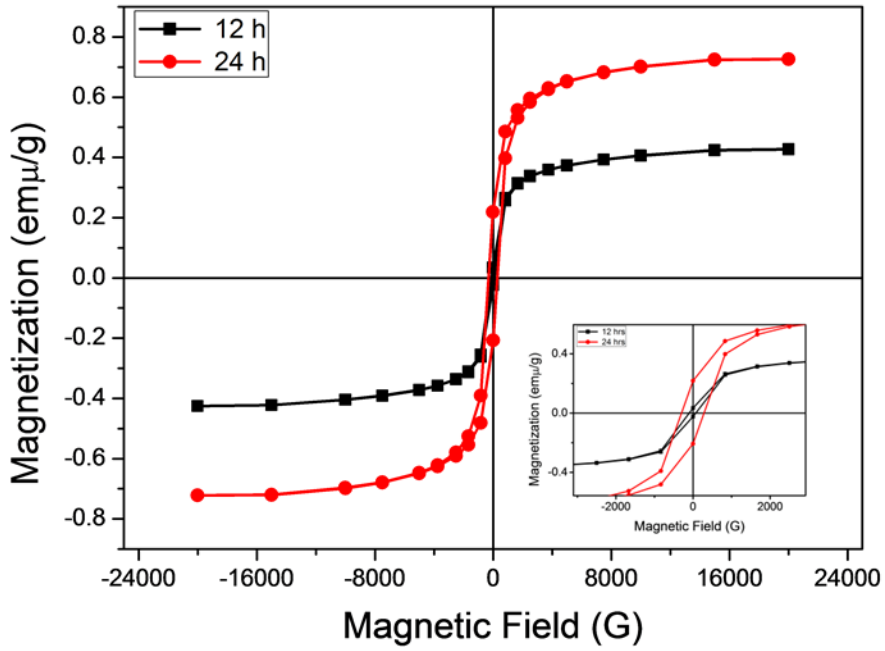
12 h
24 h
Magnetization (emμ/g)
Magnetic Field (G)
0.8
0.6
0.4
0.2
0.0
-0.2
-0.4
-0.6
-0.8
-24000
-16000
-8000
0
8000
16000
24000
12 hrs
24 hrs
Magnetization (emμ/g)
Magnetic Field (G)
0.4
0.0
-0.4
-2000
0
2000

Figure 6

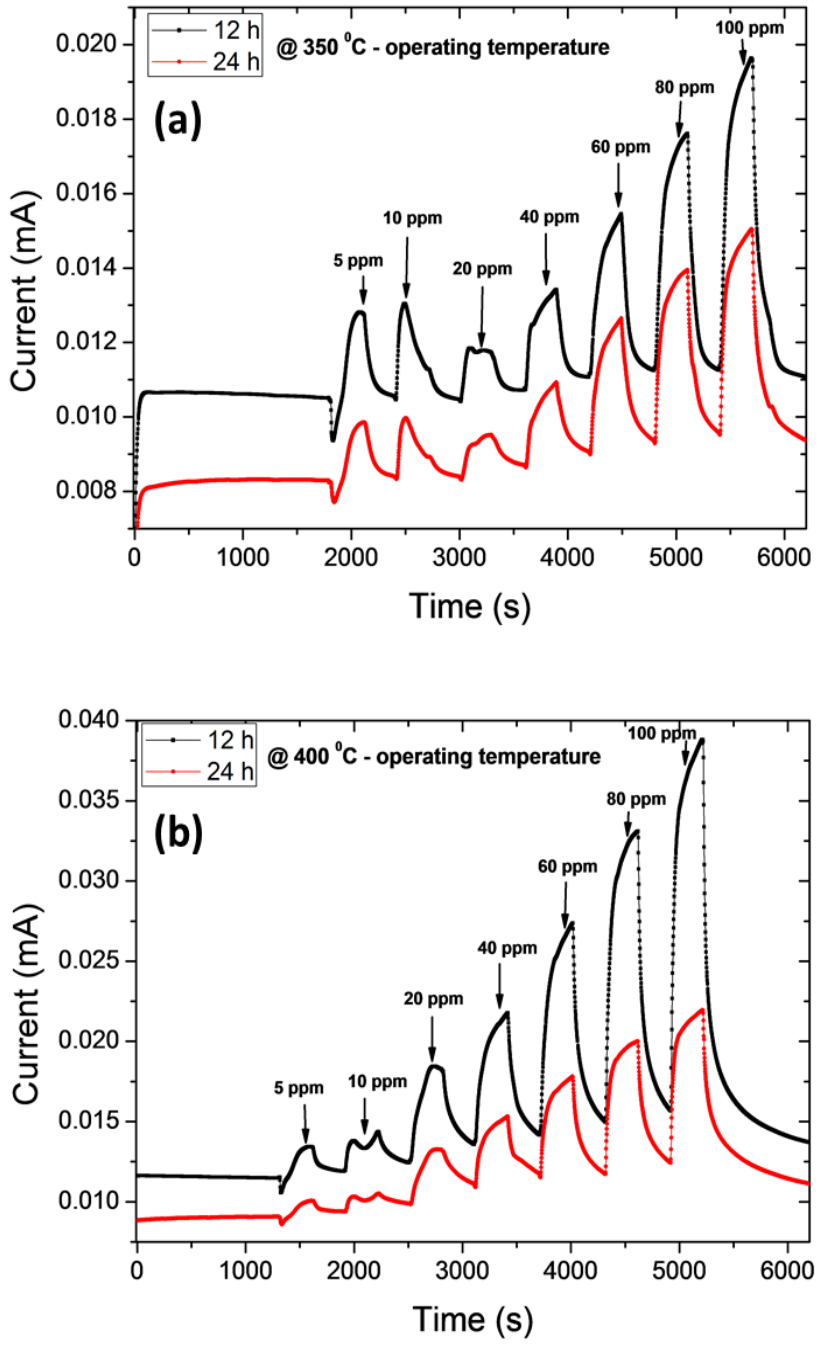
12 h
24 h
@ 350 °C - operating temperature
(a)
5 ppm
10 ppm
20 ppm
40 ppm
60 ppm
80 ppm
100 ppm
Current (mA)
Time (s)
12 h
24 h
@ 400 °C - operating temperature
(b)
5 ppm
10 ppm
20 ppm
40 ppm
60 ppm
80 ppm
100 ppm
Current (mA)
Time (s)

Figure 7

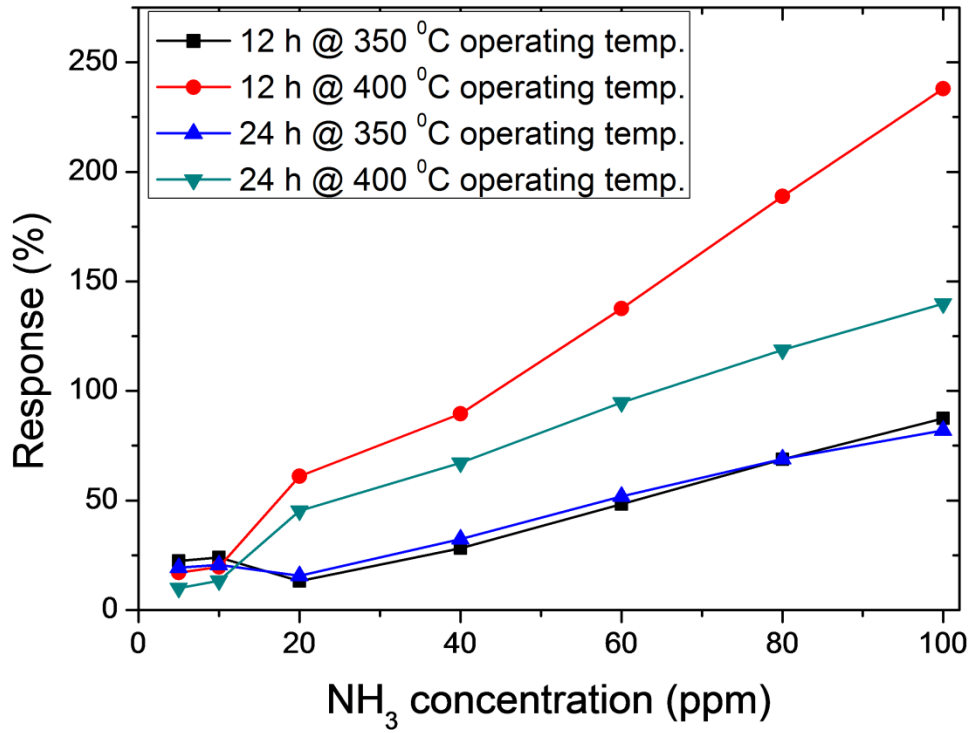
12 h @ 350 °C operating temp.
12 h @ 400 °C operating temp.
24 h @ 350 °C operating temp.
24 h @ 400 °C operating temp.
Response (%)
0
50
100
150
200
250
0
20
40
60
80
100
NH3 concentration (ppm)

Figure 8

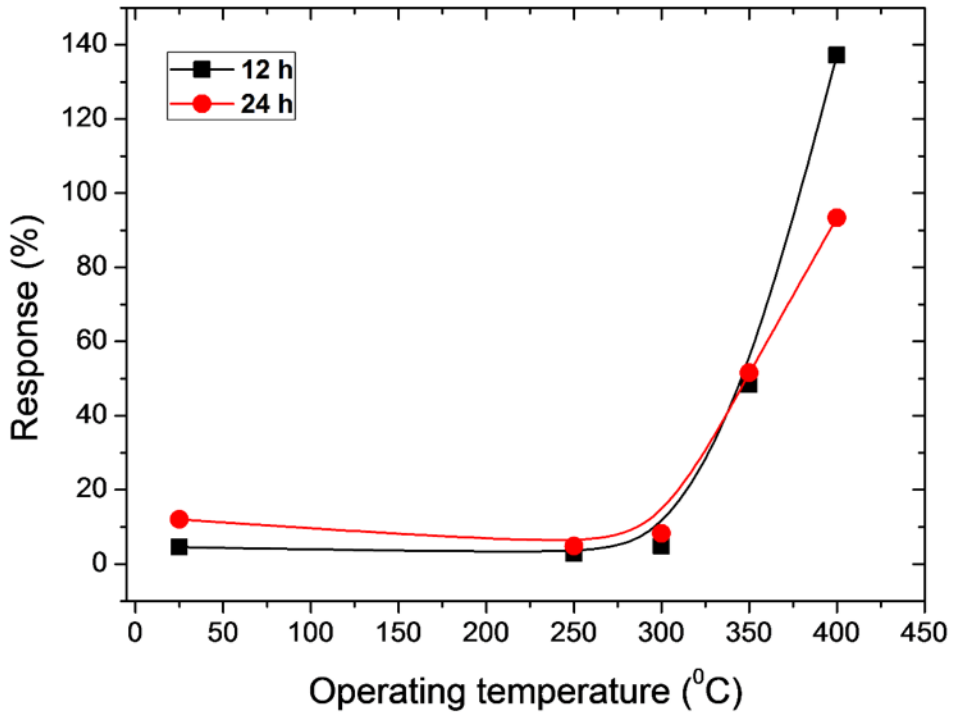
12 h
24 h
Response (%)
Operating temperature (^{0}C)
0
20
40
60
80
100
120
140
0
50
100
150
200
250
300
350
400
450

Figure 9

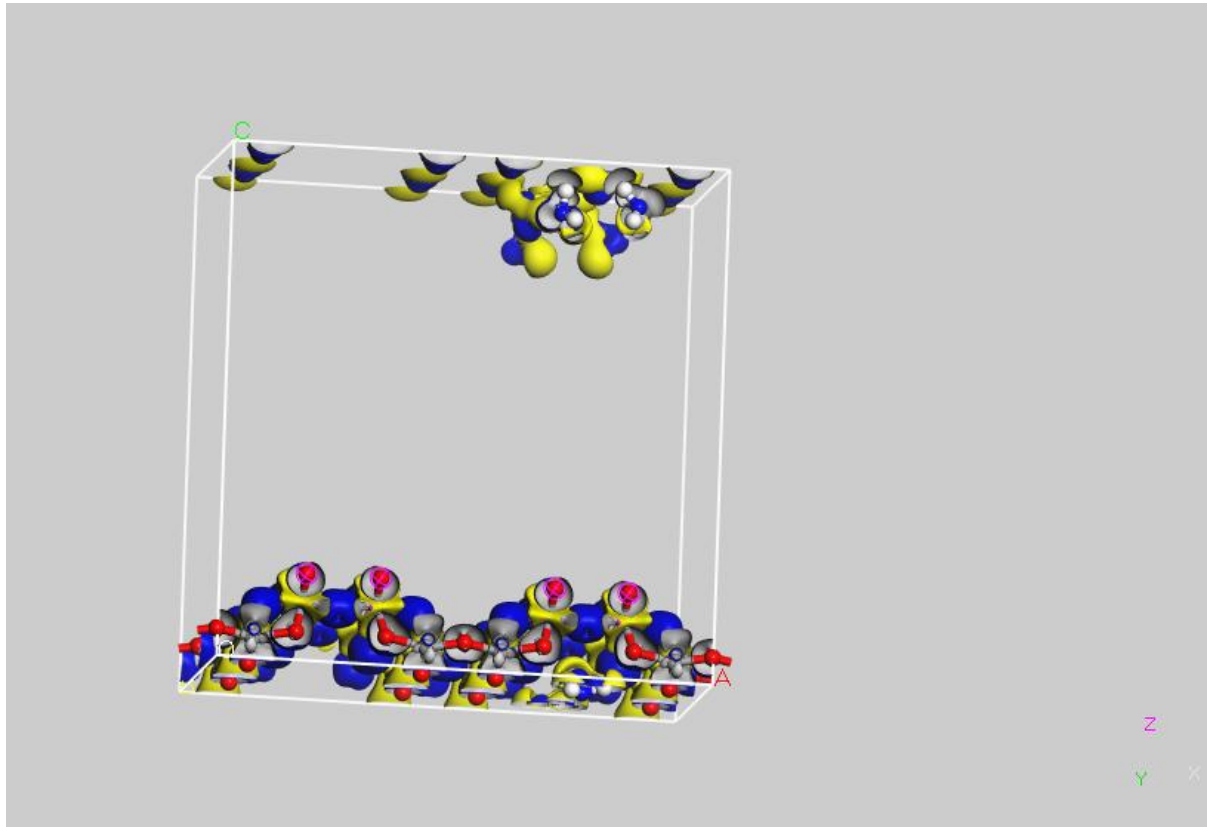

Figure 10

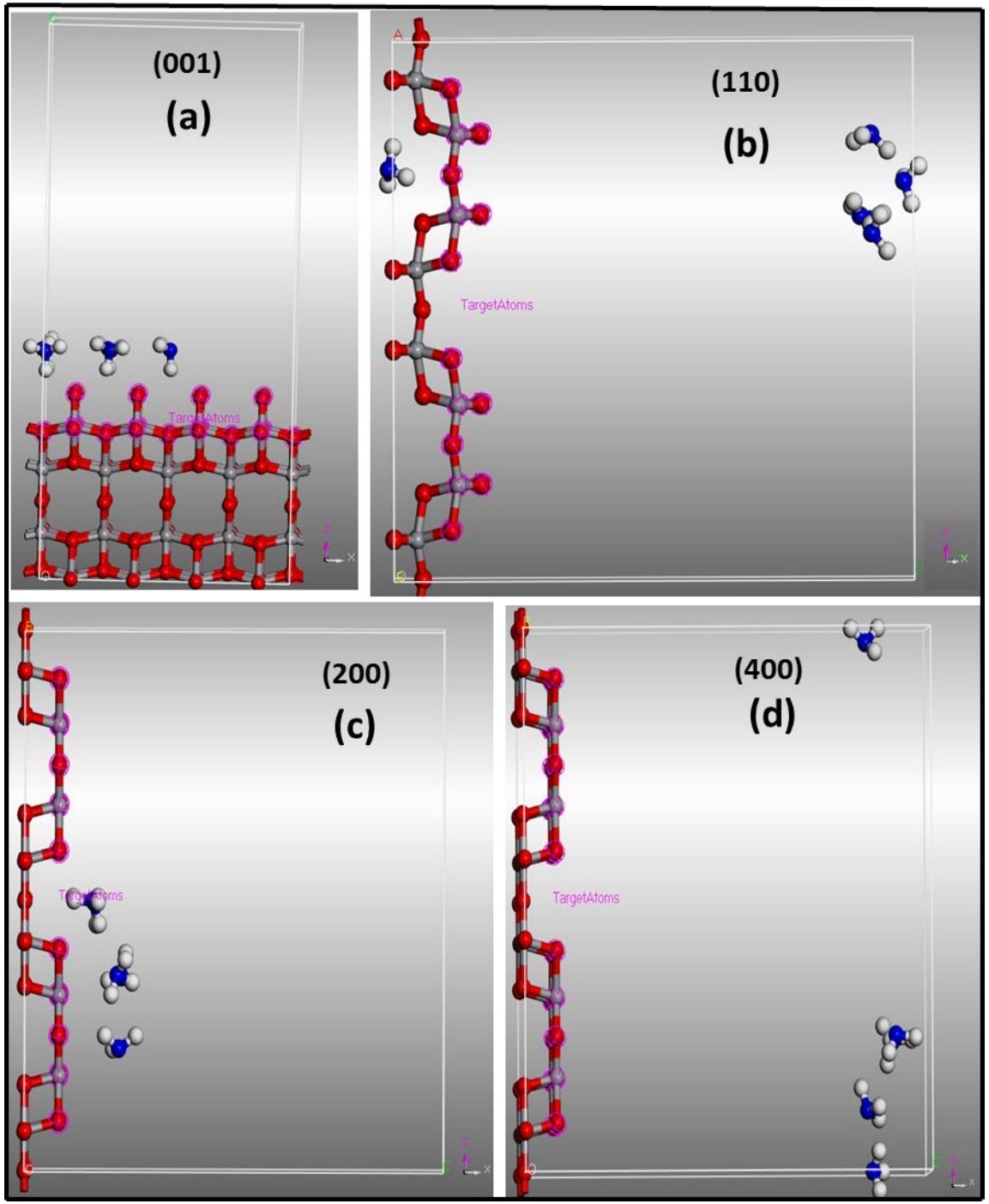
(001)
(a)
TargetAtoms
(110)
(b)
TargetAtoms
(200)
(c)
TargetAtoms
(400)
(d)
TargetAtoms

Figure 11

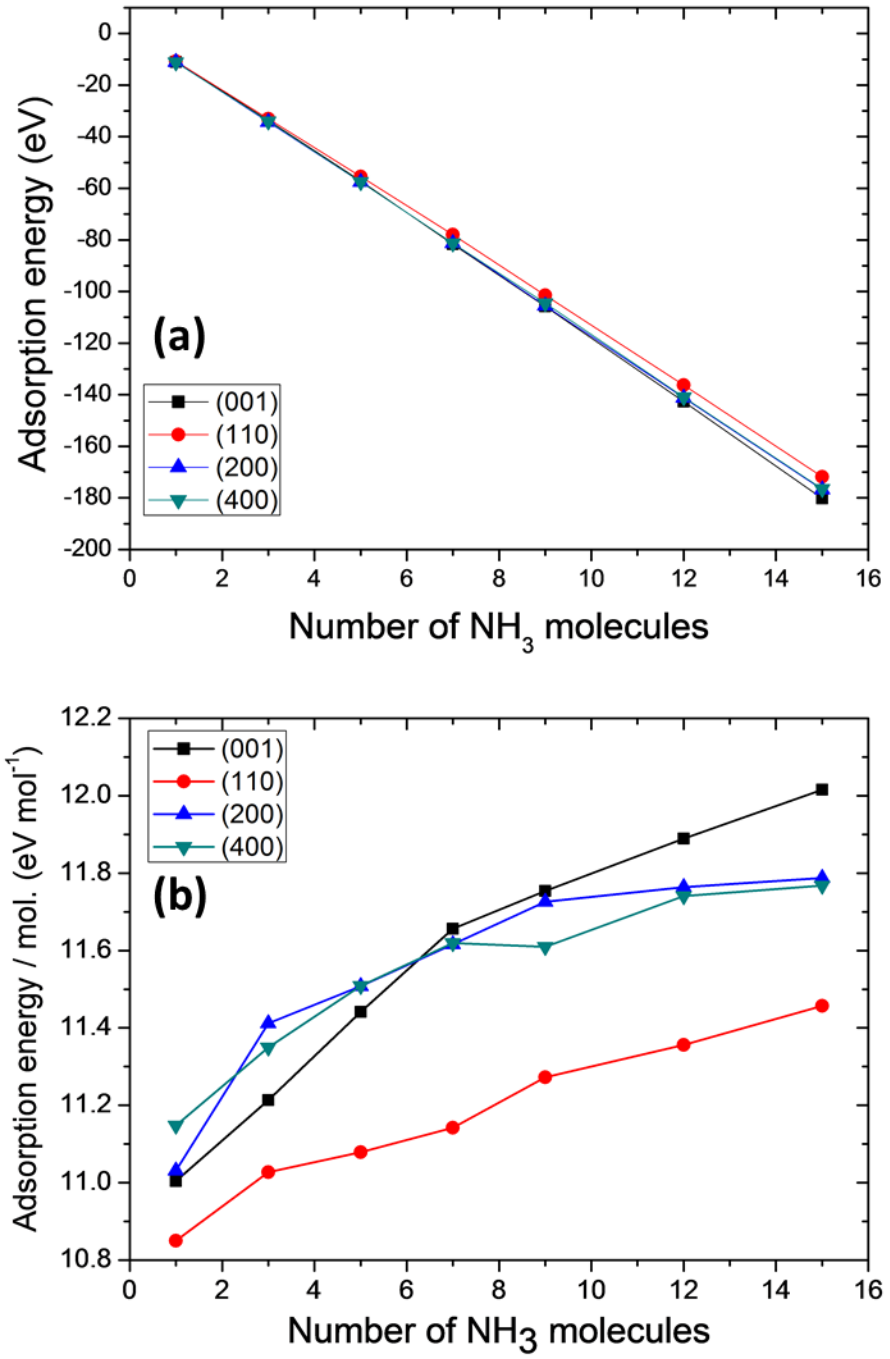
Adsorption energy (eV)
0
-20
-40
-60
-80
-100
-120
-140
-160
-180
-200
(a)
(001)
(110)
(200)
(400)
0
2
4
6
8
10
12
14
16
Number of NH3 molecules
Adsorption energy / mol. (eV mol-1)
12.2
12.0
11.8
11.6
11.4
11.2
11.0
10.8
(b)
(001)
(110)
(200)
(400)
0
2
4
6
8
10
12
14
16
Number of NH3 molecules

Figure 12

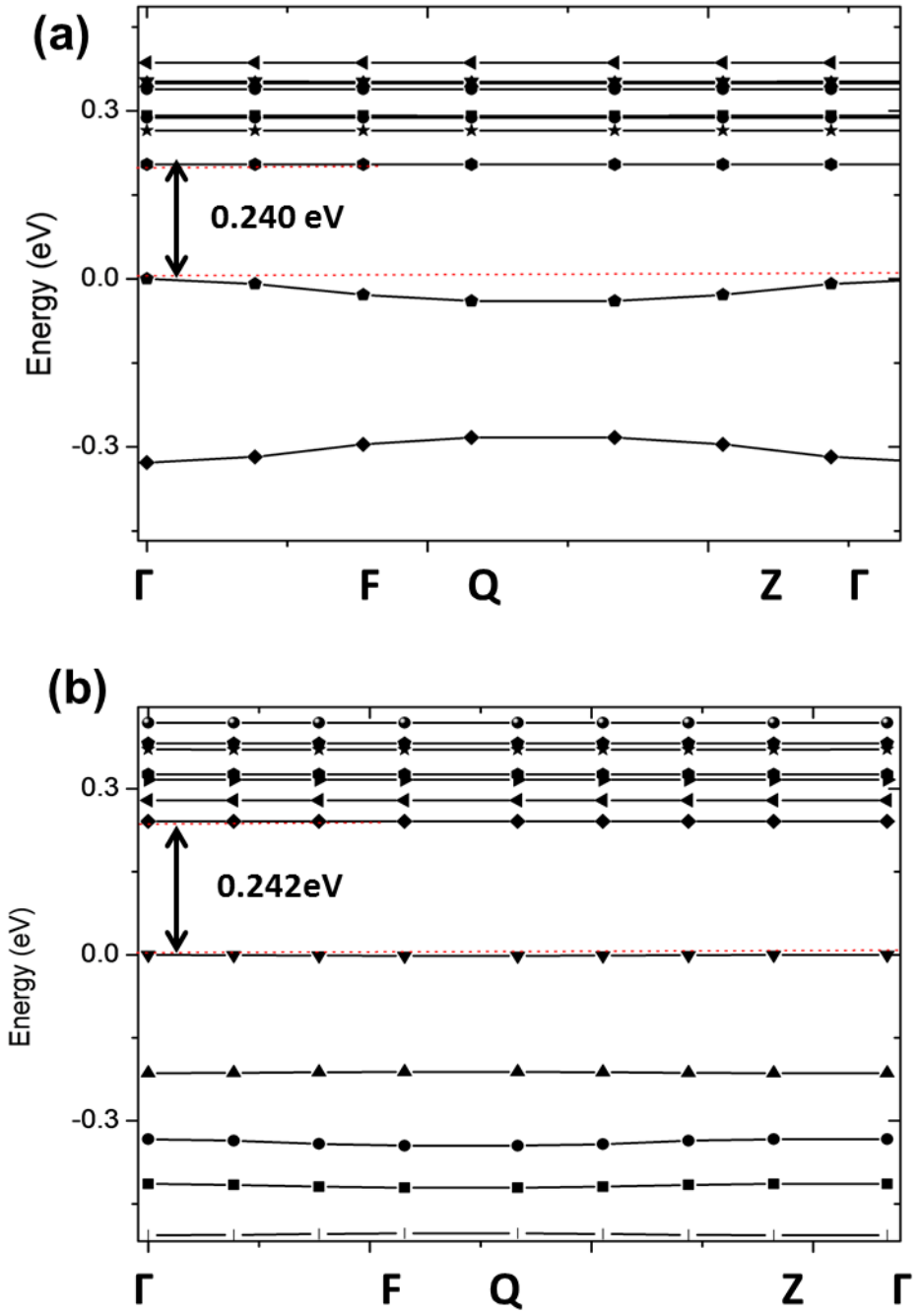
(a)
0.3
0.0
-0.3
Energy (eV)
0.240 eV
Γ
F
Q
Z
Γ
(b)
0.3
0.0
-0.3
Energy (eV)
0.242eV
Γ
F
Q
Z
Γ

Figure 13